CFD-Based Compartmental Modeling of Single Phase Stirred-Tank Reactors

Debangshu Guha, M. P. Dudukovic, and P. A. Ramachandran
Chemical Reaction Engineering Laboratory, Washington University in St. Louis, St. Louis, MO 63130

S. Mehta and J. Alvare
Air Products and Chemicals Inc., Allentown, PA 18195

DOI 10.1002/aic.10772
Published online January 24, 2006 in Wiley InterScience (www.interscience.wiley.com).

Mechanically agitated reactors are widely used in variety of process industries. Traditional designs assume perfect mixing which often fails to predict the performance of large scale industrial reactors. The effect of mixing becomes pronounced when the time scales of some of the reactions are small compared to the time scale of mixing. The objective of this work is to predict the influence of mixing on the performance of stirred-tank reactors by developing a compartmental model that incorporates the flow field simulated by CFD. This enables the coupling of the flow field, turbulent mixing and kinetics in an appropriate way, and bridges the existing gap between CFD and phenomenological models. © 2006 American Institute of Chemical Engineers *AIChE J,* 52: 1836-1846, 2006
Keywords: stirred tank, single phase, mixing, CFD, compartmental model

Introduction

Traditional design of mechanically agitated reactors, which are widely used in variety of process industries, is based on the assumption of perfect mixing. This assumption is only justified when all the reaction time scales are much larger than the mixing time scale. It often fails because perfect mixing at all length scales can never be achieved and concentration gradients do exist within the reactor over finite distances and times. This has serious consequences for scale-up of multiple reaction systems where some of the reaction time scales are small compared to the time scale of mixing. Since chemical reactions are molecular events, the product distributions can be severely affected by the concentration inhomogeneities within the reactor. As a result, the formation of undesired products can increase significantly thereby leading to increased generation of wastes.

Mixing in a stirred-tank reactor takes place through convection (at larger length scales in the inertial subrange; commonly referred to as macromixing), coarse-scale turbulent exchanges (at intermediate length scales larger than the Kolmogorov scale; commonly called mesomixing), as well as by deformation of fluid elements followed by molecular diffusion (at smaller length scales below the Batchelor scale; commonly described as micromixing).[1] In the completely turbulent regime (Reynolds number for impeller,$Re_{imp} > 10^4$) the macromixing effect on the reactor performance depends highly on the flow field that exists within the reactor. Hence, detailed flow descriptions are needed to describe the mixing effects and predict the performance in a stirred-tank reactor.

Mixing effects in stirred vessels have been traditionally addressed using phenomenological models. These models provide analysis of the effects of mixing on the product distribution and selectivity of industrial reactions in stirred reactors. Common phenomenological models include the segregated flow/ maximum mixedness models, the interaction by exchange with the mean (IEM) model,[2] the engulfment deformation diffusion (EDD) model,[3] and more recently the population balance model.[4] These models attempt to describe the effect of micromixing on the reactor performance, but none of them account for the detailed flow description within the reactor (macromixing). The other usual approach is that of compart-

Correspondence concerning this article should be addressed to M. P. Dudukovic at dudu@che.wustl.edu.

mental modeling, which essentially attempts to describe the macromixing effects on the reactor performance, and also accounts for certain level of mesomixing through the inclusion of the exchange coefficients. An example of this approach is the Network of Zones model,[5,6] which does account for the prevalent flow field inside the reactor. This model, however, depends on the available literature correlations for the impeller pumping flow (the flow number) which are needed to map the flow field in the system. It has been shown that the uncertainties in the estimation of the flow number (which varies about 30–50% when based on different literature correlations) can result in significant uncertainties in the model predictions.[7] Mesomixing is mimicked in the network of zones model, by the use of exchange flows between compartments which are taken as a fraction of the main flow through the compartment. The number of compartments and the fractions selected for estimation of the exchange flows serve as model parameters and are generally selected arbitrarily. But despite its limitations, this approach has been shown to capture the essential features of macromixing in stirred vessels operating in both batch[8] and semibatch[9] modes. The qualitative comparison of 3-D visualizations of passive tracer mixing using a colored dye showed reasonable agreement with the model predictions.[8] More recently, CFD has emerged as an alternative for the solution of reactive flow problems which can be used to solve the flow field as well as the concentration field simultaneously (or separately) in a stirred vessel.[10,11,12] However, the CFD solutions can become computationally intensive for industrial reactions and reactors where the number of components involved might be significantly large and the vessels are huge. This can be of concern for online prediction of product distribution and, hence, such an approach will not be suitable for process optimization and model based advanced control.

An improved methodology (in terms of reduced computational expense and time) can be devised if the CFD solution for the flow in the reactor is used along with the phenomenological models, thereby decoupling the flow and the kinetics of the system, but still accounting for the effect of the hydrodynamics on the mixing behavior of the system. There have been some modeling efforts along these lines recently for many types of reactors including stirred tanks[13,14,15] and bubble columns.[16] These models have been shown to produce reasonable predictions at much lower computational cost. This makes them suitable for optimization of product distribution, formulation of pollution prevention strategies and advanced model based control. The simple two-compartment model,[13] however, is still a significant simplification of the flow description within the reactor and therefore it is unlikely that the model will capture the effect of different feed locations on reactor performance. Akiti and Armenante[15] used the volume of fluid (VOF) approach to track the reaction zone and solved the reactive flow problem using the engulfment model,[3] where the engulfment parameter is calculated using the averaged turbulent parameters (k and ε) in the reaction zone. Although the qualitative trends for different feed locations are captured, quantitative comparison shows discrepancies with the experimental results. The work presented here attempts to develop the CFD-based compartmental approach, in which the complete CFD solution of the flow and turbulence parameters provides the input for the compartmental mixing model. A scheme to calculate the number of compartments necessary for a given reactive system has also been devised, based on the time scales associated with the process. The application of the model for single phase systems is shown in this article, but it can be extended to model multiphase systems as well (for example, gas-liquid or liquid-solid systems). However, it is important to recognize that this model can only account for macromixing and mixing due to turbulent dispersion, but ignores micromixing effects on reactor performance. The condition for which micromixing effects can be ignored depends on micromixing time scale compared to reaction time scale as discussed later in the text.

This article is organized as follows: the detailed model for turbulent reactive flows is described, followed by the model reduction to obtain the compartment level equations along with the assumptions involved. Then the discretization strategy and incorporation of CFD solution into the compartmental framework is described. The next section provides the results and discussions for mixing with and without reactions. Finally, the conclusions of this work are outlined.

Detailed Model for Turbulent Reactive Systems

The mass balance equation for any component c in the reactor is given by[17]

$$\frac{\partial c_c}{\partial t} + u_i \frac{\partial c_c}{\partial x_i} = D_m \frac{\partial^2 c_c}{\partial x_i^2} + R_c \tag{1}$$

Reynolds averaging Eq. 1, by decomposing the concentration as $c_c = \bar{c}_c + c_c'$ and the velocity as $u_i = \bar{u}_i + u_i'$ results in

$$\frac{\partial \bar{c}_c}{\partial t} + \bar{u}_i \frac{\partial \bar{c}_c}{\partial x_i} + \frac{\partial \overline{u_i' c_c'}}{\partial x_i} = D_m \frac{\partial^2 \bar{c}_c}{\partial x_i^2} + \bar{R}_c + \overline{R_c'} \tag{2}$$

Rendering Eq. 2 dimensionless by using a characteristic length scale L, velocity scale U_0 and concentration scale C_0 we get (* indicates dimensionless quantities)

$$\frac{\partial \bar{c}_c^*}{\partial t^*} + \bar{u}_i^* \frac{\partial \bar{c}_c^*}{\partial x_i^*} + \frac{\partial \overline{u_i'^* c_c'^*}}{\partial x_i^*} = \frac{D_m}{LU_0} \frac{\partial^2 \bar{c}_c^*}{\partial x_i^{*2}} + Da\bar{R}_c^* + Da\overline{R_c'^*} \tag{3}$$

The second term on the LHS of Eq. 3 accounts for convection due to the mean flow. The third term accounts for dispersion caused by the fluctuations. The Reynolds averaged reaction term contains the contributions from the mean reactant concentrations ($\bar{R}_c^*$), and the mean of the cross terms of the fluctuating concentrations ($\overline{R_c'^*}$). Damkohler number, Da is the ratio of the convection time scale to the reaction time scale ($Da = (L/U_0)/(C_0/R(C_0))$). The first term on the RHS accounts for the contribution from molecular diffusion. (D_m/LU_0) is the ratio of the convection time scale to the diffusion time scale, that is, inverse of the Peclet number Pe. For completely turbulent flows at high Reynolds number for liquid phase systems $Pe \gg 1$ (since $Re \gg 1$ and $Sc \gg 1$), and the contribution of molecular diffusion can be safely neglected. However, the scalar-flux term (dispersion) and the second part of the reaction term ($\overline{R_c'^*}$) need to be closed to solve the system of equations.

The scalar flux term is commonly closed using the gradient diffusion model[18] which can be written as

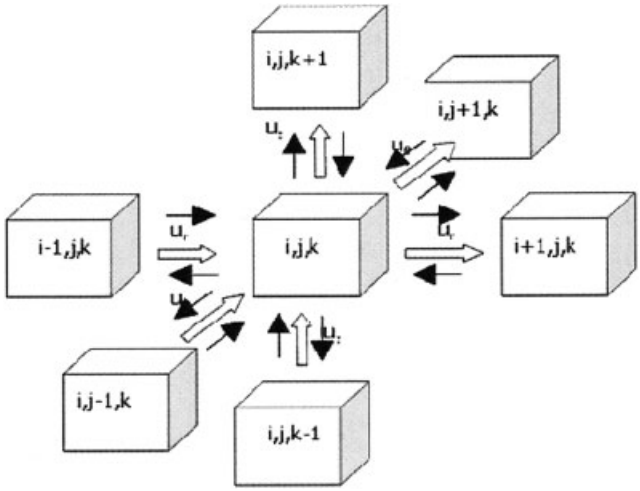

Figure 1. Configuration of a single backmixed compartment showing neighboring interconnected compartments.

$$\overline{u_i' c_c'} = -D_t \frac{\partial \bar{c}_c}{\partial x_i} \text{ or } \overline{u_i'^* c_c'^*} = -\frac{D_t}{LU_0}\frac{\partial \bar{c}_c^*}{\partial x_i^*} \tag{4}$$

where D_t is defined as the turbulent diffusivity, or the eddy-dispersion coefficient, which varies from region to region within the reactor. (D_t/LU_0) is the ratio of the convection time scale to the dispersion time scale (inverse of the dispersion Peclet number), that is, a product of the Sc_T^{-1} (turbulent Schmidt number) and $\mathrm{Re}_t^{-1}(\mathrm{Re}_t = (LU_0/\nu_t))$.

The contribution from the fluctuating concentration in the reaction term $(\overline{R_c'^*})$ is small for slow reactions ($Da \ll 1$), where the turbulent mixing will occur before the reaction can take place.[18] In other cases the reaction term can be closed using a PDF description of the scalar field. The advantage of this method is that the total contribution to the reaction term can be directly calculated from the composition PDF.[18] An example which uses the presumed PDF method is the turbulent mixer model,[1,19] which characterizes the mixture structure by solving the mixture fraction and the variance (decomposed into different components) equations for an inert tracer. The details of the different closures available for the reaction term can be found elsewhere.[20]

This differential model (Eq. 3) can be solved along with the Navier-Stokes equations to compute the concentration field within the reactor. Commercially available CFD packages like FLUENT have codes to solve these equations, based on the finite volume approach. However, as mentioned earlier, this can become computationally intensive for multiple reactions with complex chemistries. In such cases model reduction into compartments can be useful.

Model Reduction and Compartment Level Equations

The compartmental modeling approach divides the entire reactor into a number of connected, well-mixed compartments as shown in Figure 1. Model reduction for this work is then obtained by volume averaging Eq. 3 over a defined compartment (a finite control volume V), which yields

$$\frac{d}{dt^*}\int_V \bar{c}_c^* dV + \int_V \bar{u}_i^* \frac{\partial \bar{c}_c^*}{\partial x_i^*} dV + \int_V \frac{\partial \overline{u_i'^* c_c'^*}}{\partial x_i^*} dV = \int_V Da \bar{R}_c^* dV + \int_V Da \overline{R_c'^*} dV \tag{5}$$

Using the Divergence Theorem and substituting Eq. 4 for $\overline{u_i' c_c'^*}$, Eq. 5 is modified to

$$\frac{dV\langle c_c^*\rangle}{dt^*} + \int_S n_i(\bar{u}_i^* \bar{c}_c^*) dS = \int_S \frac{D_t}{LU_0} n_i \frac{\partial \bar{c}_c^*}{\partial x_i^*} dS + \int_V Da \bar{R}_c^* dV + \int_V Da \overline{R_c'^*} dV \tag{6}$$

where $\langle c_c^* \rangle$ is the volume averaged concentration in the control volume defined as $\langle c_c^* \rangle = \int_V \bar{c}_c^* dV/V$. The second term on the lefthand side of Eq. 6 can be written as $\int_S n_i(\bar{u}_i^* \bar{c}_c^*) dS = \Sigma_{k=1}^6 \langle \bar{u}_m^* \rangle_k \langle \bar{c}_{c,m}^* \rangle_k S_k$, where $\langle \bar{u}_m^* \rangle_k$, is the surface average velocity and $\langle \bar{c}_{c,m}^* \rangle_k$ is the mixing-cup average (or volumetric flow rate average) concentration on surface k of the compartment defined as

$$\langle \bar{u}_m^* \rangle_k = \frac{\int_{S_k} n_i \bar{u}_i^* dS_k}{\int_{S_k} dS_k}$$

and

$$\langle \bar{c}_{c,m}^* \rangle_k = \frac{\int_{S_k} n_i(\bar{u}_i^* \bar{c}_c^*) dS_k}{\int_{S_k} n_i \bar{u}_i^* dS_k}$$

Note that the mixing-cup average concentration ($\langle \bar{c}_{c,m}^* \rangle_k$, for all k) is equal to the volume averaged concentration ($\langle c_c^* \rangle$), only when there is no concentration gradient in the volume element.

The first term on the righthand side (dispersion term) of Eq. 6 denotes mixing due to eddy transport (mesomixing) across the cell faces. This can be written as $\int_S (D_t/LU_0) n_i (\partial \bar{c}_c^*/\partial x_i^*) dS = \Sigma_{k=1}^6 (\langle D_t \rangle_k / LU_0) \langle (\partial \bar{c}_c^*/\partial x_i^*) \rangle_k S_k$, where $\langle D_t \rangle_k$ is the surface average turbulent diffusivity and $\langle (\partial \bar{c}_c^*/\partial x_i^*) \rangle_k$ is the surface average gradient of the concentration on surface k of the compartment defined as

$$\langle D_t \rangle_k = \frac{\int_{S_k} D_t dS_k}{\int_{S_k} dS_k}$$

and

$$\left\langle \frac{\partial \bar{c}_c^*}{\partial x_i^*} \right\rangle_k = \frac{\int_{S_k} n_i D_t \frac{\partial \bar{c}_c^*}{\partial x_i^*} dS_k}{\int_{S_k} D_t dS_k}$$

Note that $\langle (\partial \bar{c}_c^*/\partial x_i^*) \rangle_k = (\partial \langle \bar{c}_{c,m}^* \rangle / \partial x_i^*)|_k$ only when there is no concentration gradient on the surface of the compartment and $(\partial \langle \bar{c}_{c,m}^* \rangle / \partial x_i^*)|_k = (\partial \langle c_c^* \rangle / \partial x_i^*)|_k = (\Delta \langle c_c^* \rangle / \Delta x_i^*)|_k$ when

there is no concentration gradient within the compartment volume as well. In this work, the compartments are assumed to be perfectly mixed which can be justified when the size of the compartments is small, and the local *Da* in each compartment is kept smaller than one. With this assumption, Eq. 6 becomes

$$\frac{dV\langle c_c^*\rangle}{dt^*} + \sum_{k=1}^{6} \langle \bar{u}_m^*\rangle_k \langle c_c^*\rangle_k S_k = \sum_{k=1}^{6} \frac{\langle D_t\rangle_k}{LU_0} \frac{\Delta\langle c_c^*\rangle}{\Delta x_i^*}\bigg|_k S_k + \int_V Da\bar{R}_c^* dV + \int_V Da\overline{R_c'^*} dV \quad (7)$$

Some comments on the role of the dispersion term are warranted here. Note that the inverse of the dispersion Peclet number appearing in Eq. 7 can be written as

$$\frac{\langle D_t\rangle_k}{LU_0} = Sc_T^{-1}\mathrm{Re}_t^{-1} = Sc_T^{-1}\mathrm{Re}_{local}^{-1}\frac{U_{local}}{U_0}$$

where U_{local} is the characteristic velocity defined for a particular compartment, and Re_{local} is the local Reynolds number based on that velocity ($\mathrm{Re}_{local} = (LU_{local}/\nu_t)$). Turbulent Schmidt number Sc_T, is taken as 0.8 for all cases. In the regions far from the impeller, Re_{local} and U_{local} are both small, and the product $Sc_T^{-1}\mathrm{Re}_{local}^{-1}(U_{local}/U_0)$ can be of O(1). In such a case, dispersion will play a significant role on the predicted results. On the other hand, near the impeller, the local Reynolds number is large ($\mathrm{Re}_{local}^{-1} \ll 1$), and the ratio ($U_{local}/U_0$) is of O(1). In those regions the relative importance of this term is small and convection dominates the mixing behavior of the system. This has been shown in the results as well, where the inclusion of the dispersion term is important when the reactant feed point is far from the impeller, but is not necessary when reactant feeding is close to the impeller.

The second term on the righthand side of Eq. 6 is the reaction term due to the mean concentration, where $\bar{R}_c^* = f(\bar{c}_c^*)$. When no concentration gradients exist within a compartment this can be written as $\int_V \bar{R}_c^*(\bar{c}_c^*)dV = \bar{R}_c^*(\langle c_c^*\rangle)V$. The third term on the righthand side (contribution from the mean of the cross terms) is neglected in this work, based on the fact that the local *Da* in each compartment is kept smaller than 1 when the reactor is discretized into compartments. Eq. 7 then gets modified to

$$\frac{dV\langle c_c^*\rangle}{dt^*} + \sum_{k=1}^{6} \langle \bar{u}_m^*\rangle_k \langle c_c^*\rangle_k S_k = \sum_{k=1}^{6} \frac{\langle D_t\rangle}{LU_0} \frac{\Delta\langle c_c^*\rangle}{\Delta x_i^*}\bigg|_k S_k + \bar{R}_c^*(\langle c_c^*\rangle)V \quad (8)$$

Equation 8 represents the mass balance for any component *c* in a compartment in dimensionless form. In terms of dimensional variables Eq. 8 can be represented as

$$\begin{aligned} V_{i,j,k}\frac{dc_c^{i,j,k}}{dt} &= c_c^{i-1,j,k}S_{rad}^{i-1}u_{rad}^{i-1,j,k} + c_c^{i,j-1,k}S_\theta u_\theta^{i,j-1,k} \\ &+ c_c^{i,j,k-1}S_{ax}u_{ax}^{i,j,k-1} - c_c^{i,j,k}S_{rad}^{i}u_{rad}^{i,j,k} - c_c^{i,j,k}S_\theta u_\theta^{i,j,k} - c_c^{i,j,k}S_{ax}u_{ax}^{i,j,k} \\ &- k_{ex}^{(i-1)}s_{rad}^{i-1}(c_c^{i,j,k} - c_c^{i-1,j,k}) - k_{ex}^{(i+1)}S_{rad}^{i}(c_c^{i,j,k} - c_c^{i+1,j,k}) \\ &- k_{ex}^{(j-1)}S_\theta(c_c^{i,j,k} - c_c^{i,j-1,k}) - k_{ex}^{(j+1)}S_\theta(c_c^{i,j,k} - c_c^{i,j+1,k}) \\ &- k_{ex}^{(k-1)}S_{ax}(c_c^{i,j,k} - c_c^{i,j,k-1}) - k_{ex}^{(k+1)}S_{ax}(c_c^{i,j,k} - c_c^{i,j,k+1}) + R_cV_{i,j,k} \end{aligned} \quad (9)$$

where, $R_c = \sum_{m=1}^{N_R} \nu_{mc}r_m$; N_R = number of reactions; r_m = intrinsic rate of the *m-th* reaction; = ν_{mc} = stoichiometric coefficient, and $k_{ex}^{(i-1)}$ = exchange coefficient at the *(i−1)* face of the compartment *(i,j,k)* which is related to D_t as shown later. Equation 9 is the final compartment level model equation used in this work.

Compartmental Model Inputs from CFD

The CFD-based compartmental model consists of the following steps. The complete CFD solution of the flow field is first obtained in the entire tank. The next step is to determine the required number of compartments depending on the time scales of the reactions studied. This is discussed in the next section. The first six terms on the RHS of Eq. 9 account for the transfer of component *c* by the bulk mean flows which are obtained by averaging the complete CFD solution over the faces of the defined compartments. The next six terms in the equation account for the transfer of mass due to turbulent dispersion. The exchange coefficient is estimated from the turbulent diffusivity averaged over the faces of the compartment as indicated later in the text.

Compartment discretization scheme

The discretization scheme followed in this work has the following objective. Given the kinetics of a reactive system, the compartments are created in such a way that the overall local residence time of the liquid in a compartment is less than the characteristic reaction time scale, that is

$$\frac{V_i}{Q_{in,i}} < t_{rxn} \quad (10)$$

where $\mathrm{V_i}$ is the volume of the *i*-th compartment, $Q_{in,i}$ is the sum of all the inlet flows to the *i*-th compartment, and t_{rxn} is the characteristic reaction time scale. This ensures that significant concentration gradients do not develop within a compartment due to reaction (ensures that in each compartment Da < 1), and, hence, compartments can be assumed to be macroscopically well-mixed.

To achieve the overall objective, discretization is done independently in each coordinate direction by choosing a velocity profile along that direction. The scheme involves the following steps:

- Selecting an appropriate velocity profile for discretization in each of the coordinate direction, that is, axial, radial and angular.
- Discretization along each coordinate direction is performed so that in each direction the individual criterion is met, that is

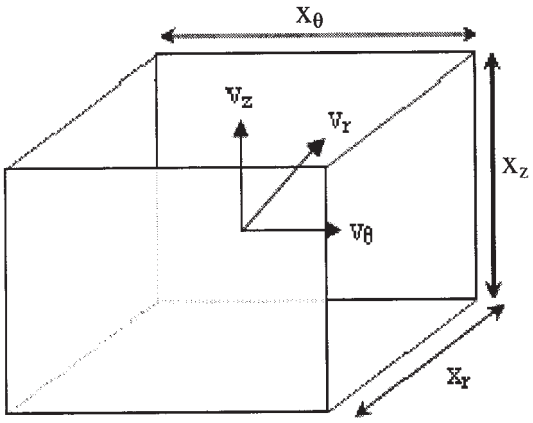

Figure 2. A discretized compartment in the compartmental framework.

$$\frac{\Delta x_i}{v_{avg}} < t_{rxn} \tag{11}$$

where v_{avg} is the average velocity between locations i and $i+1$.

Note that independent discretization in each coordinate direction essentially ensures that Eq. 10 is satisfied for about one-third of the actual reaction time scale. This follows from the scaling argument presented below. Figure 2 shows a compartment of dimensions x_r, x_z and x_θ, and three characteristic velocity components v_r, v_z and v_θ through the compartment in the three co-ordinate directions, respectively. For the given compartment

$$V \sim x_r x_z x_\theta \tag{12}$$

$$Q \sim |v_r| x_z x_\theta + |v_z| x_r x_\theta + |v_\theta| x_r x_z \tag{13}$$

$$\frac{Q}{V} \sim \frac{|v_r| x_z x_\theta + |v_z| x_r x_\theta + |v_\theta| x_r x_z}{x_r x_z x_\theta} = \frac{|v_r|}{x_r} + \frac{|v_z|}{x_z} + \frac{|v_\theta|}{x_\theta} \tag{14}$$

Now, if the discretization is carried out in each direction independently (without accounting for the contribution of the flow from the other two directions) we have

$$\frac{x_r}{|v_r|} < t_{rxn}, \frac{x_z}{|v_z|} < t_{rxn} \text{ and } \frac{x_\theta}{|v_\theta|} < t_{rxn}$$

which then implies that

$$\frac{Q}{V} > \frac{3}{t_{rxn}}$$
$$\text{or, } \frac{V}{Q} < \frac{t_{rxn}}{3} \tag{15}$$

Therefore, a reaction time scale $t'_{rxn} \sim 3t_{rxn}$ can be used for discretization, still satisfying the overall criterion given by Eq. 10.

Selecting the velocity profile

To select the axial velocity profile for discretization, circumferentially-averaged axial velocity plots (v_z $vs.z$) are obtained at different radial positions in the reactor. An average axial velocity is calculated for each of the profiles as

$$\overline{v_z}|_{r_i} = \frac{\Sigma |v_{z_i}|}{N_p} \tag{16}$$

where v_{z_i} is the velocity at any given point in the profile, and N_p is the total number of points. The average velocity obtained using Eq. 16 at each of the radial locations is compared, and the profile that has the smallest value of the mean velocity is chosen for discretization. If Eq. 11 can be satisfied for a plane which has the smallest average flow, it would satisfy the criterion at other planes also where the average flows are larger (the compartment length Δx_i remaining same).

The same procedure is followed to select the radial and tangential velocity profiles by obtaining circumferentially-averaged radial and tangential velocity plots (v_r $vs.r$ & v_τ $vs.r$) at different axial locations. The profiles with the smallest averages are chosen for discretization.

Discretization

The number and location of the axial compartments is obtained using the selected axial velocity profile. Given an axial location (Figure 3), and the corresponding velocity, we need to find a location such that

$$\frac{z_{i+1} - z_i}{\frac{1}{2}|v_{z,i+1} + v_{z,i}|} < t_{rxn} \tag{17}$$

Since the velocity profile is known, z_{i+1} can be obtained by iteration so that the earlier criterion is satisfied.

The same procedure is followed to determine the number and location of the radial compartments using the radial veloc-

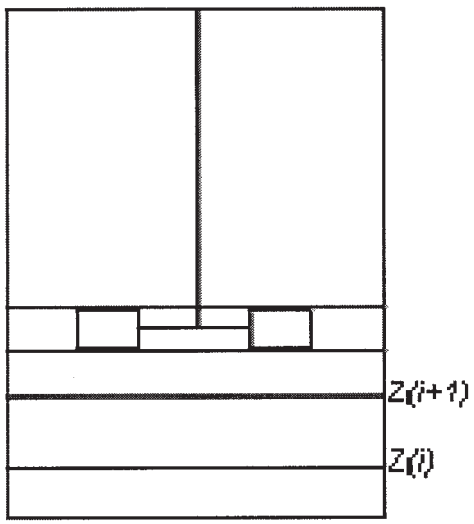

Figure 3. Discretization in the axial direction.

ity profile. The angular direction is divided evenly and the number of compartments can be obtained as

$$N_\theta = \max\left[\frac{2\pi r_i}{|v_{\theta,i}|t_{rxn}}\right] \tag{18}$$

where $v_{\tau,i}$ is the tangential velocity at r_i in the selected velocity profile.

This methodology is, however, conservative and creates too many compartments in the regions where velocities are very small (near the walls and near the bottom) and in the angular direction. This is avoided by neglecting regions of smaller velocities and dumping them into a neighboring larger compartment. The minimum velocity used in the discretization is determined from the corresponding velocity distribution (axial or radial or tangential) over the entire reactor. About 5–10% of the distribution around zero is neglected and velocities larger than that are used for discretization. Also to obtain a more realistic number of compartments, the discretization in the axial and radial direction is carried out using a larger time scale (compared to the actual reaction time scale as described earlier). The number of compartments in the angular direction is taken as a multiple of the number of impeller blades (either 6 or 12 for the cases shown). After the compartments are created it is checked if the overall objective (Eq. 10) is met.

Exchange coefficients

In earlier studies[5,6] the dispersion due to turbulence had been described by exchange flows between compartments, which were taken as a fraction of the mean flow through the compartment. In a recent work[7] this fraction has been estimated from the normalized energy dissipation rate. The dispersion term, however, accounts for a larger length scale than the length scale at which energy dissipation occurs. Using this approach to calculate the exchange parameter the exchange term near the impeller is overestimated where most of the energy dissipation occurs.[7] In this work, the exchange coefficient at each face of each compartment is represented through the turbulent diffusivity, which in turn was estimated from the kinetic energy and dissipation rates obtained from the detailed CFD simulation.

The standard k-ε model assumes isotropic turbulence and the kinetic energy of fluctuations is described as

$$k = \frac{3}{2}u'^2 \tag{19}$$

Also, the fluctuating velocity based on the same assumption of homogeneous, isotropic turbulence (Kolmogorov's Universal Equilibrium theory) can be written as

$$u' \sim (\varepsilon l_e)^{1/3} \tag{20}$$

where, ε is the dissipation rate, and l_e is the characteristic length scale.

The earlier two relationships (Eqs. 19 and 20) give an estimate of the length scale of the large eddies that account for dispersion due to turbulence. The turbulent diffusivity, which can be described as the product of the characteristic velocity and the characteristic length scale, therefore, becomes

$$D_t \sim u' l_e = A\left(\frac{k^2}{\varepsilon}\right) \tag{21}$$

The constant A can be calculated using the standard $k-\varepsilon$ model constant ($C\mu = 0.09$) and assuming $Sc_T = 0.8$, which gives $A = 0.1125$. The surface-averaged values of the turbulent diffusivity, $\langle D_t \rangle$, are obtained for each face of the compartments, and the exchange coefficient is estimated as

$$k_{ex} = \frac{\langle D_t \rangle}{\Delta x_i} \tag{22}$$

where Δx_i is the distance between the centers of two neighboring compartments in the i-direction.

Results and Discussion

The model described earlier has been used first to predict the mixing of an inert tracer in the tank. The model is then applied to single reaction schemes with linear and nonlinear kinetics to test whether it shows the effect of mixing on the performance of the reactor. The flow fields are simulated at three different impeller speeds (150, 250, and 350 RPM) with $\mathrm{Re}_{imp} \sim$ 11,000–26,000. Finally, a second-order competitive-consecutive kinetic scheme is studied.

System

The system used to simulate the flow is a cylindrical, flat-bottomed tank with diameter $T = 0.2m$. The height of the liquid is equal to the tank diameter. The tank has four baffles of width $T/10$, and is agitated by a six-bladed Rushton turbine of diameter $D = T/3$. The length of each blade is $T/12$, and the height is $T/15$. The impeller clearance (distance from the bottom of the tank) is equal to the impeller diameter. The geometry is shown in Figure 4.

Flow field

The single phase flow field is simulated using FLUENT 6.0 for the geometry shown in Figure 4. The multiple reference frame (MRF) approach[21] is used with the standard k-ε model for turbulence. The top surface of the liquid is modeled as a free surface. The physical properties of the liquid are taken as that of water.

Inert tracer mixing

The inert tracer is injected at the top free surface of the liquid near the wall as a pulse injection. The mixing time to achieve 99% homogeneity in the tank (when the concentration in each compartment is not varying more than 1% of the mean concentration) is predicted. The level of mixing achieved is monitored through the variance of the tracer concentration in the tank. Based on this, the criterion used to assure the desired level of homogeneity in the entire tank is given by

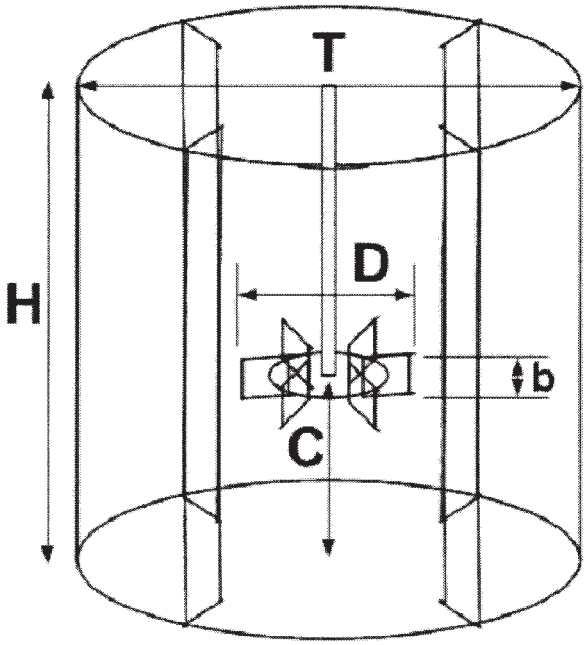

Figure 4. Geometry used.

$$\sigma \leq (1-p)\bar{c}\left(\frac{N}{N-1}\right)^{1/2} \tag{23}$$

where σ is the standard deviation defined as $\sigma = [(\sum_{i=1}^{N}(c_i - \bar{c})^2/N-1)]^{1/2}$, p is the desired degree of homogeneity, $\bar{c}$ is the mean tracer concentration when complete mixing is achieved, and N is the total number of compartments. The total number of compartments used for the simulations were varied from 120 (5×4×6:axial×radial×angular) to 720 (12×10×6: axial×radial×angular), where each of the coordinate directions is divided equally in length into the number of compartments in that direction, that is, the center to center distance between any two neighboring compartments in a given direction is same throughout the domain. The predicted mixing time decreases as the number of compartments is increased and approaches at each RPM an asymptotic value as shown in Figure 5. The convergence is achieved with 480 (10×8×6) compartments for 150 RPM, and with 432 (9×8×6) compartments for 250 and 350 RPM. Further results presented in this section have been simulated using this numbers of compartments for which mixing time convergence was achieved.

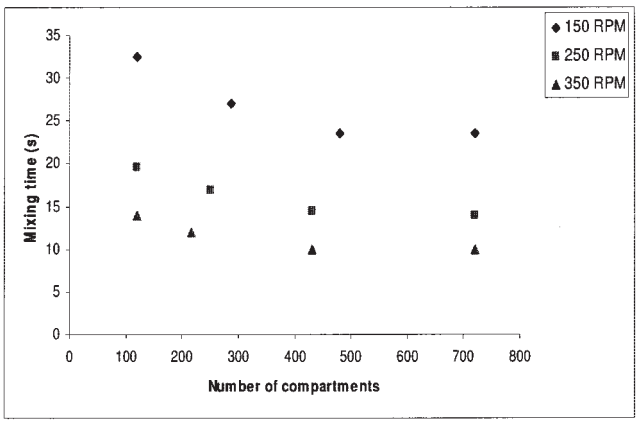

Figure 5. Convergence of predicted mixing time with number of compartments.

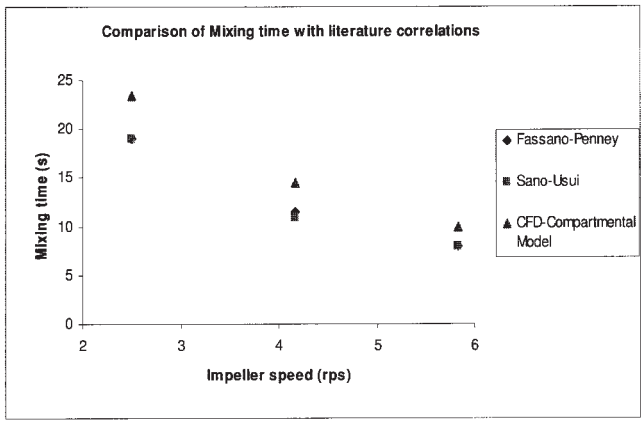

Figure 6. Predicted mixing time with literature correlations.

The mixing times predicted by the model at different impeller speeds for 99% homogeneity ($p = 0.99$) are compared with two correlations from the literature. These correlations from Fasano and Penney (1994)[22] and Sano and Usui (1985)[23] are respectively given by

$$t_m = \frac{-\ln(1-p)}{1.06N_{imp}\left(\frac{D}{T}\right)^{2.17}\left(\frac{T}{H}\right)^{0.5}} \tag{24}$$

$$t_m = \frac{3.8\left(\frac{D}{T}\right)^{-1.80}\left(\frac{b}{T}\right)^{-0.51}n_b^{-0.47}}{N_{imp}} \tag{25}$$

The constants for Eq. 24 are valid for fully turbulent regime ($Re_{imp} > 10{,}000$). At lower Reynolds number the mixing time would be greater than that predicted by this equation. For Eq. 25, all the measurements were done for $Re_{imp} > 5000$, and the constants are valid only for 99% homogeneity in the tank.

Comparison of the predicted mixing times at different impeller speeds with the two correlations is shown in Figure 6. The model predictions compared reasonably well with the correlation values to achieve 99% homogeneity in mixing. Studies on mixing in stirred-tank reactors also show that in the completely turbulent regime, the dimensionless mixing time defined as $N_{imp}t_m$ becomes constant when plotted against the impeller Reynolds number. Such a plot based on the predicted mixing time in Figure 7 also exhibits essentially a constant value. The average value of the dimensionless mixing time as predicted by the model is about 59.

First and second-order kinetics

In order to test the model developed, single reactions of first and second-order kinetics are studied at two different impeller speeds (150 and 350 RPM) for a batch system. The reaction time scale is taken as 1 s. It has to be noted that the inert mixing

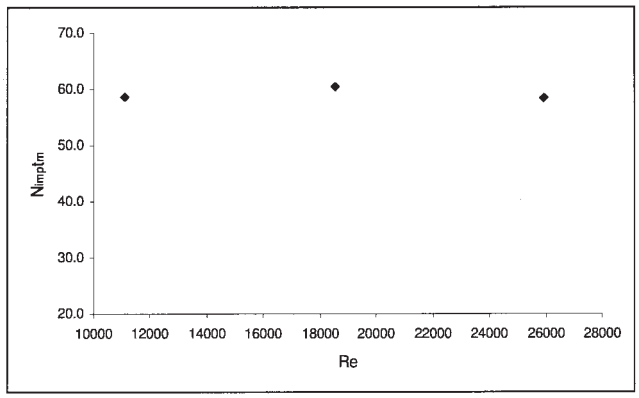

Figure 7. Dimensionless mixing time (predicted) vs. Reynolds Number.

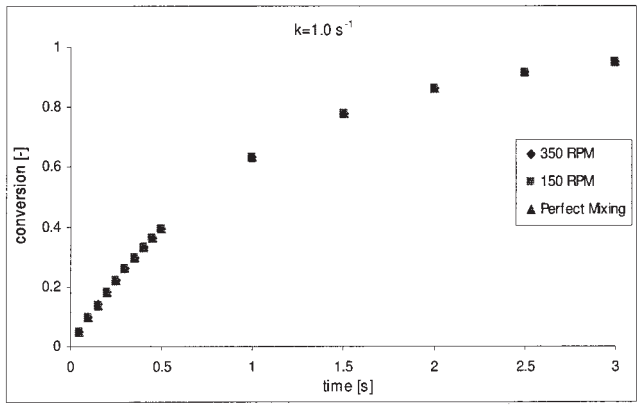

Figure 9. Conversion vs. time for a first-order reaction.

times at 150 and 350 RPM are around 19 s and 9 s, respectively, that is, the reaction time scale is kept small compared to the time scale of mixing. It is, therefore, expected that mixing should have an influence on reactor performance under these conditions.

First-order kinetics

The reaction stoichiometry for this case is given by $B \rightarrow$ *Products*. The reactant *B* is added as a pulse to solvent *A* present in the reactor. The concentration of the reactant *B* in the pulse is 100 mol/m^3, which would result in a mean *B* concentration of 10 mol/ m^3. The ratio of the added volume of reactant *B* to the total liquid volume in the reactor is ~0.1. It is assumed that the reactor volume and the flow field do not change significantly due to the addition of reactant *B*. The number of compartments used for simulation is 594 (11×9×6: axial×radial×angular) at 150 RPM and 216 (6×6×6: axial×radial×angular) at 350 RPM.

The difference in the mixing behavior of the system at different impeller speeds is visible in Figure 8, which shows a plot of the dimensionless standard deviation of the concentration of *B* in the reactor vs. conversion. The conversion is calculated based on the volume averaged mean concentration of the reactant in the reactor. The standard deviation is larger at lower impeller speed, that is, as expected mixing is poorer under this condition. On the other hand, Figure 9 shows a comparison of the reactor performance at the two speeds, and that predicted by the classical perfectly mixed-stirred tank model (instantaneous mixing at all length scales). The plots can be seen to overlap each other. This confirms the fact that conversion of a first-order reaction is always independent of the mixing behavior of the system.

Second-order kinetics

The reaction stoichiometry for this case is $A+B \rightarrow$ *Products*, and the reaction is first-order in each reactant and is second-order overall. The conditions are the same as stated in the preceding section. The mean concentration of reactant *A* already present in the reactor is 10 mol/ m^3 so that the molar ratio of the two reactants fed to the system is equal to 1.

As before, the difference in the mixing behavior at the two conditions can be observed in Figure 10. However, now the reaction kinetics being nonlinear, mixing should have an influence on reactor performance. This is shown in Figure 11. Since this is a batch process, the slower the mixing the larger is the time needed to achieve a desired level of conversion (up to 90% conversion is shown in the plot).

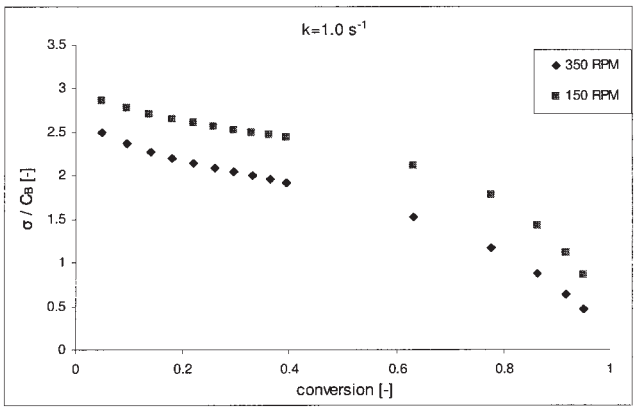

Figure 8. Dimensionless standard deviation vs. conversion for a first-order reaction.

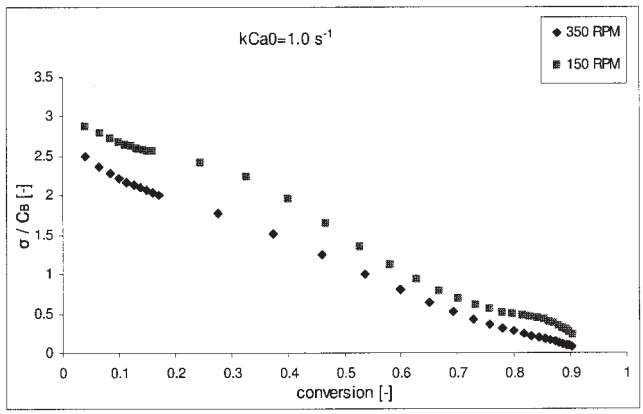

Figure 10. Dimensionless standard deviation vs. conversion for a second-order reaction.

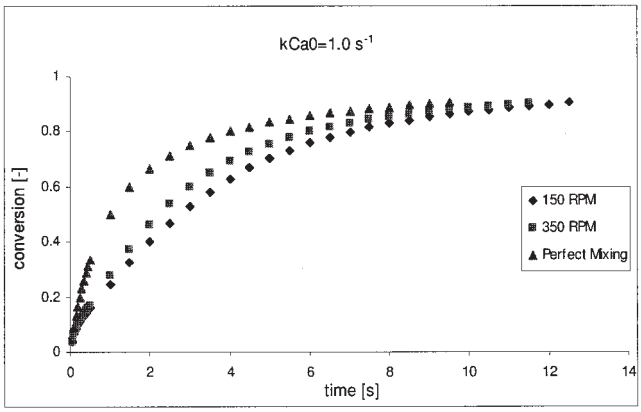

Figure 11. Conversion vs. time for a second-order reaction.

Effect of mixing on multiple reactions

Mixing effects on the performance of chemical reactors become much more significant when there are multiple reactions taking place in the system with widely varying time scales. The formation of the desired products can be increased if mixing effects in such reactions can be predicted. From an environmental point of view, this can lead to the minimization of waste generation as well.

Paul and Treybal[24] had performed experiments with a second-order, competitive-consecutive reaction scheme, and showed the effect of feed location and mixing for a homogeneous, multiple-reaction system. The reaction used in that study was the iodination (B) of L-tyrosine (A) to produce 3-iodo-L-tyrosine (R) and 3,5-diiodo-L-tyrosine (S). The reaction scheme can be written as

$$A + B \xrightarrow{k_1} R$$

$$R + B \xrightarrow{k_2} S$$

The component R is the desired product of the reaction. The kinetic constants for the two reactions, as obtained from their study at 298K, are $k_1 = 0.035\ \mathrm{m^3\ mol^{-1}\ s^{-1}}$ and $k_2 = 0.0038\ \mathrm{m^3\ mol^{-1}\ s^{-1}}$. The first reaction is an order of magnitude faster than the second reaction. These reactions are slow enough to ignore micromixing effects (as shown later) and have been used earlier to demonstrate the effect of macromixing using the Network of Zones model[25] as well.

The system comprises of semi-batch addition of reactant B (iodine) into precharged A (L-tyrosine) which has an initial concentration of $200 molm^{-3}$. The concentration of reactant B in the feed is $2000 molm^{-3}$. The feeding time for B is 15 s, and the molar ratio of reactant A to the total amount of B fed to the system is 1. The impeller speed is 1,600 RPM. The number of compartments used for simulation is 1,560 (13×10×12: axial×radial×angular). The geometry used for the experimental study is shown in Figure 12. Two feed lines were used for the addition of reactant B, one at the top and the other below the impeller. The semibatch injection of B is modeled as a series of discretized feeds at small intervals of time. The time interval between two feeds is taken as 0.5 s. No significant difference is observed by decreasing the time interval further.

An estimate of the micromixing time scale can be obtained as[26]

$$t_{micro} = 17.24\sqrt{\frac{\nu}{\bar{\varepsilon}}} \tag{26}$$

where ν is the kinematic viscosity and $\bar{\varepsilon}$ is the average kinetic energy dissipation rate given by

$$\bar{\varepsilon} = PoN_{imp}^3 D^5 V_T^{-1} \tag{27}$$

Assuming Po as 5 for a Rushton turbine operating in the completely turbulent regime, the estimated micromixing time scale for the condition simulated turns out to be ~0.007 s. The reaction time scale based on the fastest reaction can be estimated as

$$t_{rxn} = \frac{1}{k_1 \overline{C_{A0}}} \tag{28}$$

which is ~0.143 s. Since the micromixing time scale is much smaller than the time scale of the fastest reaction, performance will be limited by macromixing, and micromixing effects can be neglected.

The effect of the feed location on the mixing behavior of the system is shown in Figure 13. Mixing is poorer when the

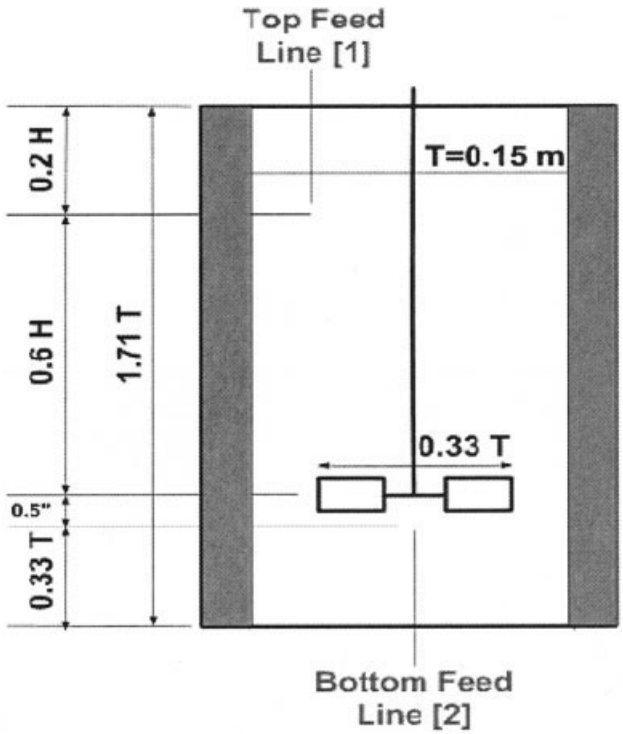

Figure 12. Details of the geometry used for the simulation of multiple reactions (Paul and Treybal[24]).

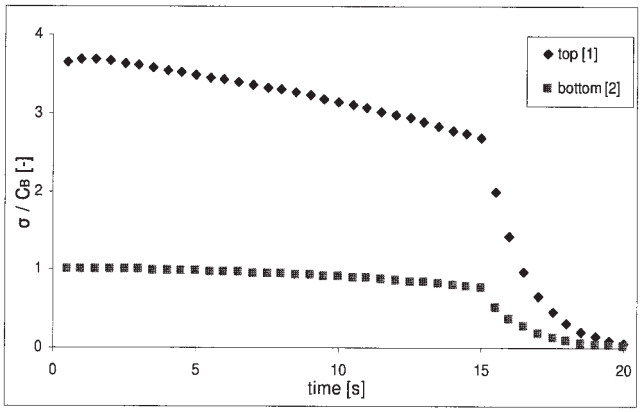

Figure 13. Dimensionless standard deviation vs. time for a semi-batch second-order, competitive-consecutive reaction scheme.

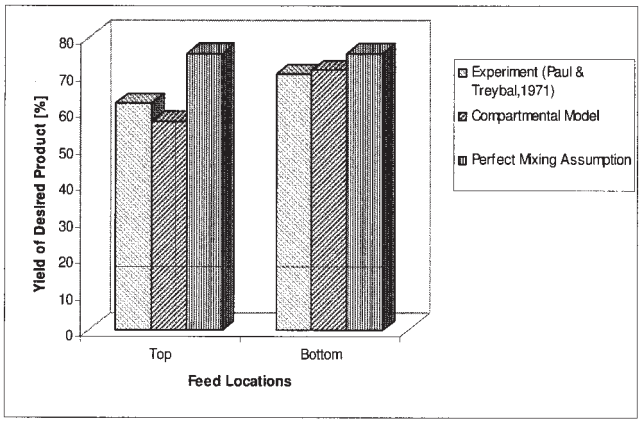

Figure 15. Comparison between measured and predicted yield of R at the end of the reaction for the two feed locations.

feeding is done from the top as evidenced by a much higher standard deviation of concentration of B compared to the bottom feed. Figure 14 shows the yield of R (defined as C_R/C_{A0}) as a function of time. The yield is lower when the top feed line is used, thereby producing more of the undesired product S due to local over-reaction.

In their experimental study, Paul and Treybal[24] measured the yield of the product R when the reaction reached completion. Figure 15 shows a quantitative comparison of the measured yield of R, and the yield predicted by the compartmental model and the perfectly mixed model at the end of the reaction for the two feed points. The conventional perfectly mixed model would predict a yield of 75.5% when there is no mixing limitation.[24] The compartmental model does a better job in predicting the product yield for different feed locations. The agreement between the experimental result and model prediction is reasonable, although the performance is slightly under-predicted for the top feed-line. Under-predicting the yield of R implies that mixing is under-predicted for that case (since poorer mixing produces less R). One of the reasons for this could be the under-estimation of the exchange coefficient term in the model equation. To check the sensitivity of the predictions to this term, simulations were done by dropping the exchange terms completely (retaining only the mean flow) and also by increasing the exchange coefficients by a factor of 2. The results are shown in Figure 16. The top-feeding turns out to be quite sensitive to the exchange term, while the bottom one is almost independent of the exchange term. This is in line with the discussion presented earlier.

Summary and Conclusions

In this work, the CFD-based compartmental model is developed and employed to predict the effect of mixing on the performance of stirred-tank reactors. The model has been shown to capture the essential features of macromixing in the reactor. For reactive systems, a discretization scheme has been developed based on the time scales of the system. The effect of the feed location on the product yield and selectivity is also captured for multiple reaction system and the results are in reasonable agreement with those experimentally observed. Based on the results obtained it can be concluded that the dispersion term (mesomixing) in the model equation is important when reactant feeding is far from the impeller. When feeding is close to the impeller, convection (macromixing) dominates, and the contribution of the dispersion term is not significant.

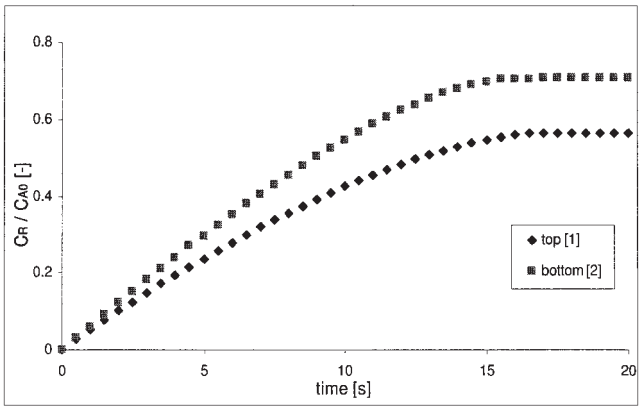

Figure 14. Yield of R as a function of time for the multiple reaction scheme.

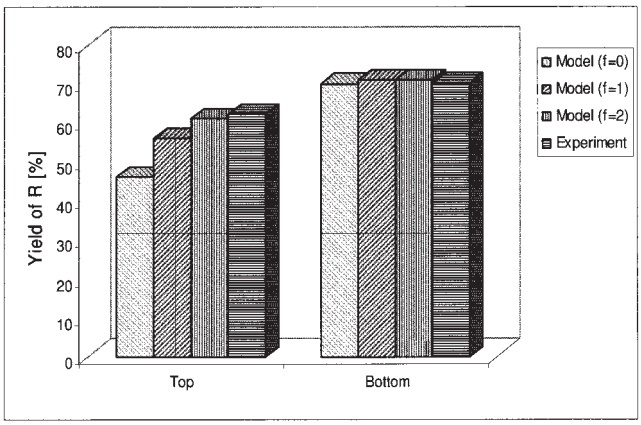

Figure 16. Sensitivity of the exchange term on the prediction of yield.

Acknowledgment

The support by the NSF-ERC award (EEC-0310689) from the National Science Foundation is hereby greatly acknowledged by the Washington University team. Additional support from Air Products and Chemicals Inc. through CREL membership is appreciated. We also appreciate the useful discussions and technical inputs from Carlos Valenzuela, Bernie Toseland and Tony Cartolano of Air Products and Chemicals Inc.

Notation

A = constant
b = blade height, m
C = clearance of impeller from tank bottom, m
c_c = concentration of component c, mol-m^{-3}
$\bar{C}_c$ = Mean concentration of component c, mol-m^{-3}
c'_c = fluctuating concentration, mol-m^{-3}
$\langle c_c \rangle$ = Volume averaged concentration, mol-m^{-3}
$\langle c_{c,m} \rangle$ = Cup-mixing concentration, mol-m^{-3}
D = impeller diameter, m
D_m = molecular diffusivity, m^2-s^{-1}
D_t = turbulent-dispersion coefficient, m^2-s^{-1}
H = liquid height, m
k = turbulent kinetic energy, m^2-s^{-2}
k_{ex} = exchange coefficient, m-s^{-1}
l_e = eddy length scale, m
n_b = number of blades
N = number of compartments
N_{imp} = impeller speed, rps
N_R = number of reactions
p = degree of homogeneity, that is, local concentrations do not vary more than (1-p)% of the mean concentration
Q = volumetric flow rate, m^3-s^{-1}
S = surface area, m^2
T = tank diameter, m
t = time, s
t_m = mixing time, s
$\bar{u}_i$ = mean velocity, m-s^{-1}
u' = Fluctuating velocity (m-s^{-1})
$\langle \bar{u}_m \rangle$ = surface average velocity (m-s^{-1})
u_{ax} = axial velocity, m-s^{-1}
u_{rad} = radial velocity, m-s^{-1}
u_θ = circumferential velocity, m-s^{-1}
V = compartment volume, m^3
V_T = total fluid volume, m^3
ε = kinetic energy dissipation rate, m^2-s^{-3}
σ = concentration standard deviation, mol-m^{-3}
ν = kinematic viscosity, m^2-s^{-1}

Dimensionless numbers

Da = Damkohler number
Pe = peclet number
Re = Reynolds number
Sc = Schmidt number
Sc_T = turbulent Schmidt number
Po = power number

Time scales

Reaction time scale: $C_0/R(C_0)$
Convection time scale: (L/U_0)
Mean residence time: (V/Q_{in})
Dispersion / mesomixing time scale: (L^2/D_t)

Literature Cited

1. Vicum L, Ottiger S, Mazzotti M, Makowski L, Baldyga J. Multi-scale modeling of a reactive mixing process in a semibatch stirred tank. *Chem Eng Sci*. 2004;59:1767.
2. David R, Villermaux J. Interpretation of micromixing effects on fast consecutive-competing reactions in semi-batch stirred tanks by a simple interaction model. *Chem Eng Commun*. 1987;54:333.
3. Baldyga J, Bourne JR. A Fluid mechanical approach to turbulent mixing and chemical reaction: II; Micromixing in the light of turbulence theory. *Chem Eng Commun*. 1984a;28:243.
4. Madras G, McCoy BJ. Kinetics and reactive mixing: Fragmentation and coalescence in turbulent fluids. *AIChE J*. 2004;50:4:835.
5. Mann R, Hackett LA. Fundamentals of Gas liquid Mixing in a Stirred Vessel: An Analysis Using Network of Back-Mixed Zones. *6th European Conference on Mixing*;1988.
6. Holden PJ, Mann R. Turbulent 3-D mixing in a stirred vessel: Correlation of a Networks-of-Zones image reconstruction approach with pointwise measurements. *IChemE Symposium Series*. 1996;140:167.
7. Boltersdorf U, Deerberg G, Schluter S. Computational studies of the effects of process parameters on the product distribution for mixing sensitive reactions and on distribution of gas in stirred tank reactors. *Recent Res Devel Chem Eng*. 2000;4:15.
8. Rahimi M, Senior PR, Mann R. Visual 3-D modeling of stirred vessel mixing for an inclined blade impeller. *Trans IchemE*. 2000;78A:348.
9. Rahimi M, Mann R. Macro-mixing, partial segregation and 3-D selectivity fields inside a semi-batch stirred reactor. *Chem Eng Sci*. 2001;56:763.
10. Smith III FG. A model of transient mixing in a stirred tank. *Chem Eng Sci*. 1997;52,9:1459
11. Brucato A, Ciofalo M, Grisafi F, Tocco R. On the simulation of stirred tank reactors via computational fluid dynamics. *Chem Eng Sci*. 2000; 55:291.
12. Bujalski JM, Jaworski Z, Bujalski W, Nienow AW. The influence of the addition position of a tracer on CFD simulated mixing times in a vessel agitated by a Rushton turbine. *Trans IchemE*. 2002;80,Part A:824.
13. Alexopoulos AH, Maggioris D, Kiparissides C. CFD analysis of turbulence non-homogeneity in mixing vessels: A two-compartment model. *Chem Eng Sci*. 2002;57:1735.
14. Bezzo F, Macchietto S, Pantelides CC. General hybrid multizonal/CFD approach for bioreactor modeling. *AIChE J*. 2003;49,8:2133.
15. Akiti O, Armenante PM. Experimentally-validated micromixing-based CFD model for fed-batch stirred tank reactors. *AIChE J*. 2004;50,3: 566.
16. Rigopoulos S, Jones A. A hybrid CFD-reaction engineering framework for multiphase reactor modeling: basic concept and application to bubble column reactors. *Chem Eng Sci*. 2003;58:3077.
17. Bird RB, Stewart WE, Lightfoot EN. *Transport Phenomena*. New York: Wiley; 1994.
18. Fox RO. Computational methods for turbulent reacting flows in the chemical process industry. *Revue De L' Institut Francais Du Petrole*. 1996;51, 2:215.
19. Baldyga J. Turbulent mixer model with application to homogeneous instantaneous chemical reactions. *Chem Eng Sci*. 1989;44,5:1175.
20. Fox RO. *Computational Models for Turbulent Reacting Flows*. Cambridge: Cambridge University Press; 2003.
21. Ranade VV. *Computational Flow Modeling for Chemical Reactor Engineering*, New York: Academic Press; 2002
22. Fasano JB, Bakker A, Penney WR. Advanced impeller geometry boosts liquid agitation. *Chem Eng*. Aug 1994;101,8:110.
23. Sano Y, Usui H. Interrelations among mixing time, power number and discharge flow rate number in baffled mixing vessels. *J of Chem Eng of J*. 1985;18:47.
24. Paul EL, Treybal RE. Mixing and product distribution for a liquid-phase, second-order, competitive-consecutive reaction. *AIChE J*. 1971,17,3:718.
25. Mann R, El-Hamouz AM. Effect of macromixing on a competitive/consecutive reaction in a semi-batch stirred vessel. *Proc Euro Conf on Mixing*; 1991.
26. Assirelli M, Bujalski W, Eaglesham A, Nienow AW. Study of micromixing in a stirred tank using a Rushton turbine: Comparison of feed positions and other mixing devices. *Trans IchemE*. 2002;80,Part A:855.

Manuscript received Jun. 8, 2005, and revision received Nov. 30, 2005.